Quantum Path Interferences in High-Order Harmonic Generation

A. Zaïr,* M. Holler, A. Guandalini, F. Schapper, J. Biegert,† L. Gallmann, and U. Keller
Physics Department, ETH Zurich, CH-8093 Zurich, Switzerland

A. S. Wyatt, A. Monmayrant,‡ and I. A. Walmsley
Clarendon Laboratory, Parks Road, Oxford OX1 3PU, United Kingdom

E. Cormier
CELIA, CNRS-CEA-Université Bordeaux1, 351 cours de la libération, 33405 Talence, France

T. Auguste, J. P. Caumes, and P. Salières
Service des Photons, Atomes et Molécules, CEA-Saclay, 91191 Gif-sur-Yvette, France
(Received 24 July 2007; published 10 April 2008)

We have investigated the intensity dependence of high-order harmonic generation in argon when the two shortest quantum paths contribute to the harmonic emission. For the first time to our knowledge, experimental conditions were found to clearly observe interference between these two quantum paths that are in excellent agreement with theoretical predictions. This result is a first step towards the direct experimental characterization of the full single-atom dipole moment and demonstrates an unprecedented accuracy of quantum path control on an attosecond time scale.

DOI: 10.1103/PhysRevLett.100.143902 PACS numbers: 42.65.Ky, 32.80.Wr, 42.50.Hz, 42.65.Re

High-order harmonic generation (HHG), leading to the production of extreme ultraviolet (XUV) emission by interaction of an intense laser field with an atomic or molecular target, has become intensely studied [1], in particular, for the generation of isolated [2,3] and trains [4,5] of attosecond pulses. The underlying physics is well described by the semiclassical three-step model [6,7], in which an electron initially in the ground state is freed into the continuum by tunnel ionization, accelerated, and ultimately driven back to the core by the oscillating linearly polarized laser field where it may recombine and emit a high-energy harmonic photon. A quantum-mechanical theory has been developed within the strong field approximation (SFA) [8,9]. Similar to the Feynman's path integral approach, the harmonic dipole moment can be written as the sum over different quantum path contributions to the XUV emission. These quantum paths are a generalization of the classical electron trajectories. The phase $\phi_q^{(j)}$ associated to each quantum path (j) of harmonic order q is given by the classical action along the corresponding trajectory, and can be approximated by the product of the ponderomotive energy U_p with the electron excursion time $\tau_q^{(j)}$: $\phi_q^{(j)} \approx -U_p \tau_q^{(j)} \approx -\alpha_q^{(j)} I$, where I is the laser pulse intensity and $\alpha_q^{(j)}$ is roughly proportional to $\tau_q^{(j)}$. The longer the trajectory, the stronger the intensity dependence of the associated dipole phase. The relative phase between the different trajectories leads to interference in the total single-atom dipole moment. This generic behavior is illustrated in Fig. 1 for harmonic 15 generated in argon (solid black curve). The calculated dipole strength exhibits fast oscillations with increasing intensity when the harmonic is in the plateau region, where many quantum paths contribute to the emission. At low intensity when the harmonic enters the cutoff, the interferences disappear due to only a single quantum path contributing. When the harmonic dipole is restricted to the two shortest orbits, referred to as the short ($\tau_q^{(1)} \approx T/2$, $\alpha_q^{(1)} \approx 1$–5×10^{-14} rad cm^2/W) and long ($\tau_q^{(2)} \approx T$, $\alpha_q^{(2)} \approx 20$–$25 \times 10^{-14}$ rad cm^2/W) trajectories (T is the laser period) [8], regular oscillations are observed (red curve in Fig. 1) with an average period of 0.3×10^{14} W/cm^2 close to the expected $2\pi/\Delta\alpha$ interference period of the two first quantum paths (first order quantum path interferences, QPI). These fast oscillations are smoothed out if integrated over laser intensities varying by a small amount in the order of $2\pi/\Delta\alpha$. In the experimental conditions of a gas jet positioned in the focus of an ultrashort laser beam, the spatial and temporal averaging will smear out these oscillations in the macroscopic response (dotted curve in Fig. 1). Indeed only monotonic, unmodulated distributions have been measured up to now [10,11]. While the contributions from the two main quantum paths have been independently characterized experimentally [12–16], their relative phase is still unknown since no direct observation of their interference has been reported so far.

In this Letter, we show that we can theoretically define, and experimentally find, conditions where the QPI are directly observable. In order to avoid temporal averaging, we perform spectral filtering, while spatial averaging is partly avoided through far-field spatial filtering. The latter also allows one to balance the weight of the two quantum path contributions to increase the interference contrast. The measured contrast is high enough to resolve the QPI over all the generated plateau harmonics. This gives access

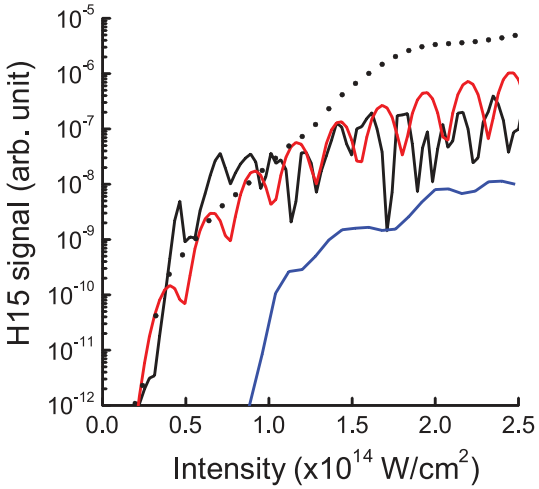

FIG. 1 (color). Calculated argon 15th harmonic: single atom dipole strength including all quantum paths (black curve) and restricted to the two shortest quantum paths (red curve); macroscopic response without filtering (black dot curve) and with off-axis spatial filtering (blue curve, far-field filtering from 14 to 20 mrad).

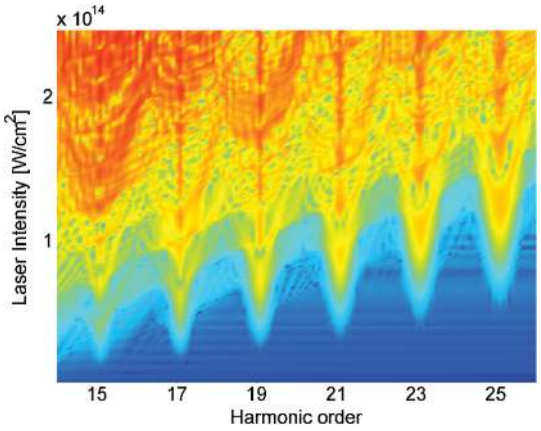

FIG. 2 (color). Single argon atom harmonic spectra as a function of peak laser intensity for a 30-fs pulse duration.

to the relative quantum paths phase that is needed to reconstruct the single-atom dipole moment and get insight into the ultrafast electronic dynamics in the emission process. Moreover, by slightly changing the laser intensity, we demonstrate a control of these paths on an attosecond time scale. Indeed, only tiny changes (of a few 10 as) of the electron trajectories are enough to shift their relative phase by π.

Let us first consider temporal averaging effects due to the pulse envelope. We can get around them by using the temporal variation of the dipole phase that induces a chirp of the harmonic emission through a phase modulation process [17–20]: $\Delta\omega(t) = \frac{\partial \phi_q^{(j)}(t)}{\partial t} = \alpha_q^{(j)} \times \frac{\partial I(t)}{\partial t}$. This chirp, and thus the harmonic spectral bandwidth, increases with laser intensity. However, if one considers the signal precisely at the harmonic central frequency, it always corresponds *in time* to the maximum of the laser temporal envelope, while the emission from the envelope edges is shifted to different side frequencies (i.e., the harmonic chirp effectively maps time to frequency $\Delta\omega = \omega - \omega_q$). By spectrally resolving the harmonic, we thus get rid of the temporal averaging. Even if the chirp is larger for the long trajectory contribution than for the short one, the spectral bandwidth where the two contributions overlap is generally large enough to allow detection of harmonic yield modulations. This is illustrated in Fig. 2, which shows the argon single-atom harmonic spectrum as a function of peak laser intensity. These SFA simulations are performed for a 30 fs (FWHM) Gaussian laser pulse at 800 nm. At each harmonic central frequency, the yield is modulated with the peak laser intensity due to first-order QPI and the harmonic spectral width increases as expected. On either side of the central harmonic frequency, a parabolic shape of the harmonic spectral distribution is visible. Typically in this region the long trajectory dominates the HHG process but also a few percent of the short trajectory still contribute and may induce a fringe pattern with a low contrast. Some additional fine structure is also visible in this region, especially for low order harmonics; this is due to higher-order QPI and phase modulation effects. We also performed simulations based on the solution of the time-dependent Schrödinger equation (TDSE) in the single active electron approximation, using a model atomic potential [21]. The results confirm our observations and highlight the robustness of the interference effects.

Let us now turn to spatial averaging effects. Averaging along the propagation direction can be reduced by using a generating medium shorter than the laser confocal parameter. As for the transverse averaging, we may use the spatial analog of the temporal or spectral filtering. The intensity dependence of the dipole phase leads to a curvature of the harmonic phase front (equivalent to a spatial chirp) [17,19,20,22]: the (near-field) distribution at the exit of the medium is "projected" into the far field so that a far-field spatial selection can prevent transverse spatial averaging. However, an additional difficulty arises here due to different phase matching of the two quantum paths [23]. We obviously need generating conditions where both paths give significant contributions to the macroscopic response. This implies focusing the laser after the generating medium. In this situation, the short path is phase matched on axis, and the long path off axis. This results in a concentration of the short (long) path contribution at the center (outskirts) of the far-field profile. The two trajectories relative contribution thus varies radially, and there is an optimum position off axis where the QPI fringe contrast will be maximum. A far-field spatial filter positioned there will in addition limit the spatial averaging. The importance of this spatial selection for the QPI observation is demonstrated by simulations of the full macroscopic response using the SFA dipole and a three-dimensional propagation code that solves the propagation equations for the laser and harmonic fields in the paraxial and adiabatic approxima-

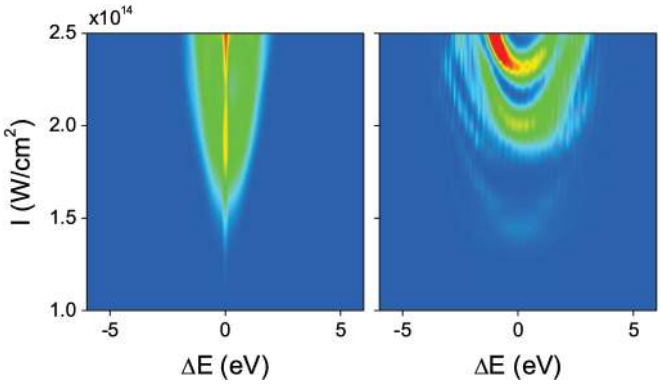

FIG. 3 (color). Calculated macroscopic spectra of the argon 15th harmonic as a function of peak laser intensity without (left) and with (right) a far-field 6-mrad off-axis window. The harmonic signal is plotted with a linear color scale defined as blue at zero strength to red at maximum strength (10^{10} without window and 4.5×10^7 with window).

tions. The generating conditions are a 30 fs laser pulse is focused 3 mm after a 1 mm long, 10 Torr argon gas jet, with a confocal parameter of 12 mm. The harmonic spectrum was calculated after propagating the harmonic electric field to the far field where we applied spatial filtering along one dimension: a 6 mrad wide integration window centered 17 mrad off axis. Figure 3 shows the simulation results for harmonic 15 as a function of the *peak* laser intensity with and without the spatial selection. In the latter case (left curve), the integration is performed over the total spatial profile, but the main contribution comes from the 6-mrad central part. The spatial averaging results in blurring of the QPI and therefore the harmonic amplitude is not modulated, but the spectral width still increases with the peak laser intensity as expected. In contrast, when the far-field selection is performed (right curve), the harmonic spectrum reveals a clear parabolic shape similar to those observed in the single-atom response in Fig. 2. The fringes contrast is maximum at the harmonic central frequency ($\Delta E = \hbar \Delta \omega = 0$), as expected for the first-order QPI. The fringes are shifted to higher peak laser intensity when $|\Delta E|$ increases because these frequencies are generated on the edges of the laser temporal envelope and thus correspond to a smaller effective intensity. This could explain the parabolic shape of the QPI. We have observed a similar behavior for all plateau harmonics. The fine structures visible in the SFA single-atom response are here smoothed out by the macroscopic response. Note finally that the harmonic signal is reduced by 1 to 2 orders of magnitude when the spatial selection is performed, which makes the experimental observation of QPI challenging.

In the experiments, we used a Ti:sapphire laser system delivering 30 fs, 800 nm pulses at a repetition rate of 1 kHz with a maximum pulse energy of 1.5 mJ. The laser beam is focused by a 50 cm radius of curvature (ROC) spherical mirror into a pulsed argon jet. A half wave plate and a polarizer are used to precisely and continuously control the peak intensity in the jet from 0.5×10^{14} W/cm^2 to 4.5×10^{14} W/cm^2. The high-harmonic emission is reflected by a gold spherical mirror (ROC = 30 m) under grazing incidence at the entrance of a spectrometer composed of a platinum grating and a backside-illuminated CCD. The gold mirror can be transversally moved to spatially select a part of the beam, acting as a spatial window with an acceptance angle of 6 mrad that can be moved from perfect on-axis alignment to an off-axis position. The gas jet is positioned 3 mm before the laser focus to phase match both quantum paths. The acquisition of each harmonic spectrum is performed over 5000 laser shots. High-energy stability is thus required to ensure that QPI is not smeared out due to intensity fluctuations. Figure 4 shows the harmonic spectra acquired as a function of peak laser intensity at the center of the jet. It was estimated from the intensity at focus measured by recording the focal spot, pulse duration and energy. In Fig. 4(a), on-axis selection is performed, such that the short trajectory contribution dominates. As expected, the harmonics are spectrally narrow and their amplitudes saturate monotonically with laser intensity. Very similar spectra are obtained when the jet is positioned 3 mm after the focus, in a condition where only the short quantum path is phase matched. In Fig. 4(b), off-axis selection is performed. Because of the filtering, the harmonic signal is reduced by 1 order of magnitude. A clear broadening of the plateau harmonics (from order 13 to 25) is visible, consistent with the long trajectory contribution as observed in [14]. At a sufficiently high intensity, neighboring harmonics start to overlap. If the laser carrier-envelope offset phase (CEP) was stabilized [24–26], one would observe interferences between long path contributions from both orders generated at different times of the laser envelope [13]. In our experiments, the CEP was random so that these interferences were blurred out and did not perturb the observation of the first-order QPI. The latter does not depend on the laser CEP since it occurs on the subcycle attosecond time scale. The amplitudes of the plateau harmonics are clearly modulated as a function of peak laser intensity. The parabolic structures observed in the calculation are clearly visible in the experimental data and the fringe periodicity ($\sim 0.3 \times 10^{14}$ W/cm^2 at the harmonic central frequency) coincides with the calculated value for the first-order QPI. Other possible sources of spectral distortions cannot explain the observed behavior. Ionization starts to play a role around 2.5×10^{14} W/cm^2 (argon saturation intensity) and induces an asymmetry in the calculated and measured spectra at high intensity. Changes in phase matching may also occur with increased intensity, but they are not expected at lower intensities where the parabolic shapes first appear. Finally, the strong phase modulation of the long trajectory may alone produce spectral interferences due to the emission of the same frequency at two different instants of the laser temporal intensity profile. However, in this case, the spectrally integrated harmonic signal (integrated over a single harmonic) would not show any modulation upon varying the laser

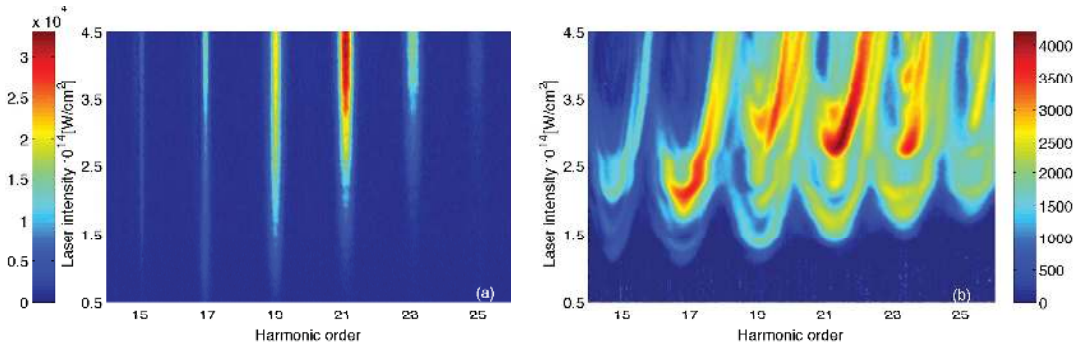

FIG. 4 (color). Measured harmonic spectral dependence on the peak laser intensity with far-field 6-mrad spatial filtering. (a) on-axis filtering; (b) off-axis filtering.

peak intensity. This is in contrast to our measured and simulated spectra, as is shown in Fig. 1 where the H15 spectrally integrated but spatially filtered signal still exhibits modulations (blue curve), though with a reduced contrast due to the remaining temporal averaging. At the exact harmonic frequency, the above-mentioned spectral interferences do not occur, since emission of this frequency happens at a single instant in time.

In conclusion, we have observed for the first time the interference between the two shortest quantum paths contributing to the harmonic emission. Spectral and far-field spatial filtering allow us to minimize the temporal and spatial averaging that otherwise blurs out the interference in the macroscopic response. This interference is not CEP sensitive since it occurs on the subcycle time scale of the quantum paths. By varying the laser intensity, we change their relative phase and thus demonstrate a paths control on an attosecond time scale. Indeed, at 1.5×10^{14} W/cm^2, a 10% intensity variation shifts the QPI from constructive to destructive interference for harmonic 15 which in saddle-point calculations corresponds to extremely small variations in excursion times for both quantum paths: $\Delta\tau_{15}^{(1)} = -22$ as and $\Delta\tau_{15}^{(2)} = +13$ as. The resulting attosecond emission is shifted in time by similar amounts, demonstrating the possibility for unprecedented accuracy in the control of attosecond pulses. Our experiments are also a first step towards the direct measurement of the full single-atom dipole. Longer quantum paths are predicted by the SFA and TDSE calculations and their interferences appear as fine structure in the single-atom harmonic spectra. These higher-order QPIs may become observable in the macroscopic response by means of our detection technique, in particular, in neon or helium, when several higher-order trajectories could contribute significantly to the HHG process [27] while ionization effects will be limited. Finally, the high sensitivity of our interferometric technique will be particularly useful for the investigation of trajectory behavior in HHG taking place in more complex systems such as molecules or clusters.

This research was supported by the NCCR Quantum Photonics (NCCR QP), research instrument of the Swiss National Science Foundation (SNSF), the U.K. Attoscience Consortium (EPSRC GR/S24015/01), the French Agence Nationale de la Recherche (ANR-05-BLAN-0295-01, ATTO-SCIENCE), COST-STSM-P14-01910, the European support RTN XTRA (MRTN-CT-2003-505138), and the Conseil Régional d' Aquitaine (M3PEC-UBx1). The authors thank A. L'Huillier, G. Sansone, and M. B. Gaarde for stimulating discussions.

*zair@phys.ethz.ch
†Present address: ICFO, 08860 Castelldefels (Barcelona), Spain.
‡Present address: LAAS-CNRS, 31077 Toulouse Cedex 4, France.

[1] P. Agostini and L. F. DiMauro, Rep. Prog. Phys. **67**, 813 (2004).
[2] M. Hentschel *et al.*, Nature (London) **414**, 509 (2001).
[3] G. Sansone *et al.*, Science **314**, 443 (2006).
[4] P. M. Paul *et al.*, Science **292**, 1689 (2001).
[5] Y. Mairesse *et al.*, Science **302**, 1540 (2003).
[6] P. B. Corkum, Phys. Rev. Lett. **71**, 1994 (1993).
[7] K. Schafer *et al.*, Phys. Rev. Lett. **70**, 1599 (1993).
[8] M. Lewenstein, P. Salières, and A. L'Huillier, Phys. Rev. A **52**, 4747 (1995).
[9] P. Salières *et al.*, Science **292**, 902 (2001).
[10] J. J. Macklin *et al.*, Phys. Rev. Lett. **70**, 766 (1993).
[11] C.-G. Wahlström *et al.*, Phys. Rev. A **48**, 4709 (1993).
[12] J. Mauritsson *et al.*, Phys. Rev. A **70**, 021801(R) (2004).
[13] G. Sansone *et al.*, Phys. Rev. A **73**, 053408 (2006).
[14] E. Benedetti *et al.*, Opt. Express **14**, 2242 (2006).
[15] H. Merdji *et al.*, Phys. Rev. A **74**, 043804 (2006).
[16] C. Corsi *et al.*, Phys. Rev. Lett. **97**, 023901 (2006).
[17] P. Salières *et al.*, Phys. Rev. Lett. **74**, 3776 (1995).
[18] Z. Chang *et al.*, Phys. Rev. A **58**, R30 (1998).
[19] M. B. Gaarde *et al.*, Phys. Rev. A **59**, 1367 (1999).
[20] P. Salières *et al.*, Adv. At. Mol. Opt. Phys. **41**, 83 (1999).
[21] E. Cormier and P. Lambropoulos, Eur. Phys. J. D **2**, 15 (1998).
[22] C. Lyngå *et al.*, Phys. Rev. A **60**, 4823 (1999).
[23] Ph. Balcou *et al.*, Phys. Rev. A **55**, 3204 (1997).
[24] H. R. Telle *et al.*, Appl. Phys. B **69**, 327 (1999).
[25] D. J. Jones *et al.*, Science **288**, 635 (2000).
[26] A. Apolonski *et al.*, Phys. Rev. Lett. **85**, 740 (2000).
[27] M. B. Gaarde and K. Schafer, Phys. Rev. A **65**, 031406 (2002).